Nonlinear Model Predictive Control of Photovoltaic-Battery System for Short-Term Power Dispatch

Yang Li[1*], D. Mahinda Vilathgamuwa[1], San Shing Choi[1], Troy W. Farrell[2], Ngoc Tham Tran[1], and Joseph Teague[2]
[1]School of Electrical Engineering and Computer Science, Queensland University of Technology, Brisbane, Australia
[2]School of Mathematical Sciences, Queensland University of Technology, Brisbane, Australia
Email: *y245.li@qut.edu.au, mahinda.vilathgamuwa@qut.edu.au, sanshing.choi@qut.edu.au, t.farrell@qut.edu.au, ngoctham.tran@hdr.qut.edu.au, joe.teague@qut.edu.au

***Abstract*— The paper focuses on developing power flow control strategy for electricity end users installed with photovoltaic-battery systems. The control objective is to reduce the overall cost to the end users while meeting the users' load demands. By taking into consideration the cost associated with the degradation of the battery, a nonlinear model predictive control technique is used to determine the short-term power exchange with the external grid system. The formulated nonlinear optimization problem is solved using dynamic programming technique, and an algorithm is developed to reduce the computational load. Numerical examples show the efficacy of the proposed method.**

Keywords*— *Battery energy storage system, lithium-ion battery, battery degradation, PV, model predictive control, dynamic programming.

I. INTRODUCTION

In recent years, photovoltaic (PV) panels have been widely deployed worldwide in the pursuit to achieve low-carbon electricity generation. In Australia, the number of households equipped with rooftop PV panels has reached 1.74 million in 2017, accounts for about 1/5 of the residences [1]. However, as the penetration level of the renewable distributed generation increases, the intermittent nature of solar irradiance can pose severe technical challenges to the distribution network, in the form of voltage fluctuation and overload in distribution feeders, among other issues [2]. Such negative impacts would offset the economic and environmental benefits obtained from the free and clean energy resource. Fortunately, with the help of distributed energy storage devices such as lithium-ion (Li-ion) batteries, the afore-mentioned issues can be alleviated and even completely overcome. Energy market mechanisms can be used to bring further economic benefits to the distributed generators.

In such distributed generator systems, the end users become electricity producers as well as consumers, the so-called "prosumers". A prosumer can be an individual household, a commercial building, or a microgrid in a broader sense. By regulating the battery power, the local demand can be met while the prosumer can undertake electricity power/energy exchange with the external grid. The viability and reliability of such a system rely critically on the efficacy of the energy management system to govern the power flows between generations, loads, storage, and the external grid. The design of such an energy management system is a challenging task because of the uncertainties in the renewable generations and loads.

Large amount of works have been reported pertaining to various aspects of the prosumers' energy management systems. For example, the authors of [3] have proposed a number of household appliance models but they did not explore the possibility in which a prosumer can sell electricity back to the grid. In [4], the authors proposed a bi-directional plug-in hybrid electric vehicle charging/discharging model, although the degradation effect of the battery was not considered. The formulated optimization problems in these works are often solved using linear programming or mixed-integer linear programming techniques. Unfortunately, these techniques could fail to yield the solutions because electrochemical battery is a highly-nonlinear device. Indeed, literature [5] proposed a nonlinear predictive control strategy for residential buildings. Empirical battery model with predetermined degradation parameters were used in the study. However, the parameters were obtained under battery operating conditions which may be significantly different from that encountered in practice.

The present investigation differs in a number of ways in comparison with the cited works. In particular, a physics-based dynamic model of Li-ion battery is used in which the major battery degradation mechanisms have been considered in the design of the control strategy. It then allows the prosumer to optimally determine the trading schedule based on the predicted load, solar irradiance and tariff information. The optimal power flow is determined by a nonlinear model predictive control (MPC) method, where the optimization problem is solved by a modified form of dynamic programming (DP). Furthermore, it is envisaged the future distribution energy market would be flexible and dynamic. Thus, this work assumes the prosumer would be permitted to submit its dispatch schedule to the distribution system operator (DSO) ahead of time. This will allow the DSO to arrange and schedule load, generation, storage and tariff to achieve optimal network control and management.

II. SYSTEM CONFIGURATION AND MODEL

A. System Configuration

In this section, the overall configuration and mathematical model of each component in the proposed energy management system are presented. The schematic diagram of a prosumer with PV panels and battery packs is shown in Fig. 1. The PV panels and the battery packs are connected to a dc network via the corresponding dc/dc converters, and their combined power is converted to single-phase ac form to supply the local non-deferrable loads. The net difference between the PV-battery output and the local load is compensated by the power exchange with the utility grid.

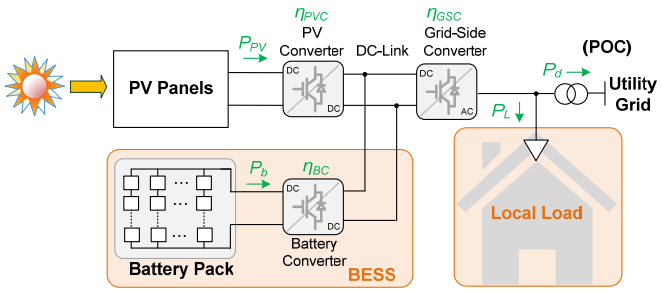

Fig. 1. Schematic diagram of a prosumer equipped with PV and battery pack.

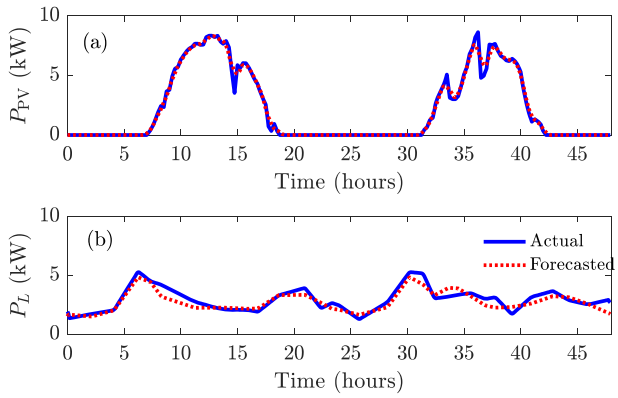

Fig. 2. Examples of (a) P_{PV} and $P_{PV,f}$ and (b) P_L and $P_{L,f}$

In Fig. 1, P_{PV}, P_b, P_L and P_d denote the harnessed PV power, battery pack power, non-deferrable local load and the power flow to grid respectively. The arrows indicate the reference direction of the power flows and P_d is referred to as the dispatched power in this work.. Power balancing demands that

$$\eta_{GSC}[\eta_{PVC}P_{PV}(t)+\eta_{BC}P_b(t)]=P_d(t)+P_L(t) \tag{1}$$

where η_{PVC}, η_{BC} and η_{GSC} represent the energy conversion efficiencies of the PV converter, the battery converter, and the grid-side converter respectively. Note that should P_b and (P_L +P_d) flow in the opposite direction to that of the reference directions, η_{BC} and η_{GSC} will be the reciprocal of the actual efficiencies of corresponding converters. For simplicity, the efficiencies are assumed constant.

B. PV Panel Power and Load

For short-term dispatch planning by the prosumer, forecasted $P_{PV}(t)$ is required. Various techniques have been applied in forecasting $P_{PV}(t)$ using either historical data, real-time measurement or geographical /meteorological information [6]. As the proposed method to be described in this paper is not dependent of the forecasting techniques used, the forecast error e_1 is assumed to be normally distributed [7], i.e.,

$$P_{PV,f}-P_{PV}=e_1\sim N(\mu_1,\sigma_1^2) \tag{2}$$

where $P_{PV,f}(t)$ denotes the forecasted $P_{PV}(t)$. The mean (μ_1) and standard deviation (σ_1) are affected by the forecasting horizon. As an illustration, $P_{PV}(t)$ at 5-minute sample rate and the corresponding one-day-ahead forecast are shown in Fig. 2(a).

Similar to $P_{PV}(t)$, the local load demand $P_L(t)$ is also assumed to be forecasted based on certain established technique. The forecasted error e_2 is again assumed normally-distributed with mean value μ_2 and the standard deviation σ_2. Typical $P_L(t)$ and its forecast $P_{L,f}(t)$ are shown in Fig. 2(b).

$P_{PV}(t)$, and to some extent $P_L(t)$, can vary beyond the control of the prosumer. Thus, in order to achieve accurate performance evaluation, the sampling rate of $P_L(t)$ and $P_{PV}(t)$ needs to be sufficiently high and in line with the complexity of the battery model which will be discussed next.

C. Li-Ion Battery Model

Li-ion battery is assumed to be the energy storage element in the prosumer because its specific power and energy densities suit amicably the present application. The cost of battery has also decreased rapidly in recent years. As battery degradation will be one major consideration in this study, a physics-based single particle model (SPM) of Li-ion battery is selected. This is because: 1) compared to empirical models, the degradation mechanisms can be more accurately described and predicted from the basic working principles of electrochemistry; 2) For stationary power applications where the battery current rate is low (commonly under 1C), SPM is accurate and requires much less computation than other electrochemical battery models.

By approximating the solid-phase diffusion using a two-parameter model, the governing equations of the SPM for a Li-ion battery cell are similar to that derived in [8], i.e.

$$\dot{c}^{\pm}_{s,\text{avg}}(t)=-\frac{3}{R_p^{\pm}}j_n^{\pm}(t) \tag{3}$$

$$c_{ss}^{\pm}(t)-c_{s,\text{avg}}^{\pm}(t)=-\frac{R_p^{\pm}}{D_s^{\pm}}\frac{j_n^{\pm}(t)}{5} \tag{4}$$

$$j_n^{\pm}(t)=\pm\frac{i(t)}{Fa^{\pm}L^{\pm}}=\pm\frac{i(t)}{F(3\varepsilon_s^{\pm}/R_p^{\pm})L^{\pm}} \tag{5}$$

$$\Phi_{s0}^{\pm}(t)=\text{OCP}^{\pm}(x_{ss}^{\pm}(t))+\eta_s^{\pm}(t)\pm\frac{r_f^{\pm}(t)}{a^{\pm}L^{\pm}}i(t) \tag{6}$$

$$\eta^{\pm}(t)=\frac{2R_gT_{\text{cell}}}{F}\sinh^{-1}\left(\frac{\pm i(t)}{2a^{\pm}L^{\pm}r_{\text{eff}}^{\pm}\sqrt{c_{e0}(c_{ss}^{\pm}(t))(1-c_{ss}^{\pm}(t))}}\right) \tag{7}$$

$$V(t)=\Phi_{s0}^{+}(t)-\Phi_{s0}^{-}(t)+r_{\text{col}}i(t) \tag{8}$$

$$I(t)=A_{\text{cell}}i(t) \tag{9}$$

where $c_{s,\text{avg}}$ and c_{ss} are the average and the surface concentration of the lithium ions in the particle. j_n, η_s, Φ_{s0}, i, I, and V are the pore-wall molar flux, the overpotential of the electrochemical reaction, the electrode potential, the applied charging current density, the applied current and terminal voltage respectively. In (6), the equilibrium potential of the main electrochemical reaction, or the open-circuit potential (OCP), is a nonlinear function of the surface stoichiometry x_{ss} = $c_{ss}/c_{s,\text{max}}$ and it is governed by the characteristics of the materials of the electrode. The mathematical expression for OCP(x_{ss}) and the physical meanings of the constant parameters D_s, a, ε_s, R_p, F, L, R_g, T_{cell}, c_{e0}, r_{eff}, $c_{s,\text{max}}$, r_{col}, A_{cell} are given in Appendix A.

For practical applications, the battery coulomb capacity ($Q^{\pm}_{\text{max}}$) and state-of-charge (SOC) are used and are defined as

$$Q_{\text{max}}^{\pm}(t)=\mp FAL^{\pm}\varepsilon_s^{\pm}c_{s,\text{max}}^{\pm}(t)(x_{100\%}^{\pm}-x_{0\%}^{\pm})/3600 \tag{10}$$

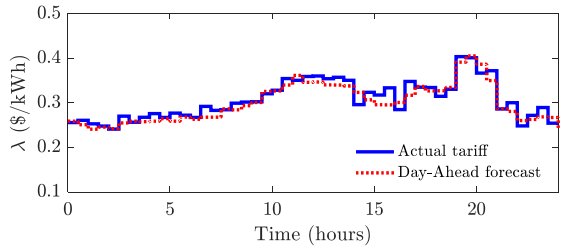

Fig. 3. An example of the hourly actual and day-ahead forecasted tariff.

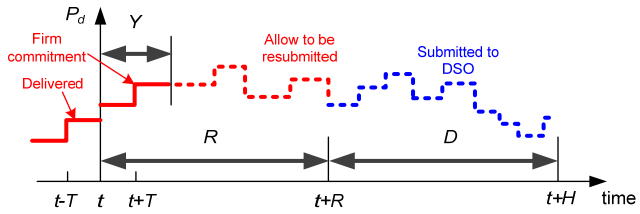

Fig. 4. Prevailing market rule within the time horizon [t, t+H].

$$\mathrm{SOC}^{\pm}(t)=\frac{Q^{\pm}_{\max}(t)(x^{\pm}_{s,\mathrm{avg}}(t)-x^{\pm}_{100\%})}{Q^{\pm}_{\max,0}(x^{\pm}_{100\%}-x^{\pm}_{0\%})}+1 \tag{11}$$

where $x_{s,\mathrm{avg}} = c_{s,\mathrm{avg}}/c_{s,\max}$. $Q_{\max}(t)$ and $Q_{\max,0}$ are the capacity of the electrode at time t and at the pristine state (i.e. new battery). Note each equation in (3)–(11) actually represents two equations: one for the positive electrode and one for the negative electrode, and the corresponding quantities are denoted by the superscript "+" and "–", respectively.

Next, two major degradations are considered: that of the irreversible increase of the resistance r_f of solid-electrolyte interphase (SEI) layers on the surface of the electrodes, and the decrease of the electrode capacity $Q_{\max}$ over time. The change of r_f and $Q_{\max}$ are caused by the side-reaction, and such side-reaction is dominant at the negative electrode [9]. So in the remaining part of this manuscript the superscript "–" is omitted to simplify notation: i.e. SOC = SOC$^-$, $Q_{\max} = Q^-_{\max}$, $r_f = r_f^-$. Furthermore, it is shown in [10] that the corresponding rates of change of $Q_{\max}$ and r_f and are

$$\dot{Q}_{\max}(t)=f_1(\mathrm{SOC},I)<0 \quad [\mathrm{Ah/s}] \tag{12}$$

$$\dot{r}_f(t)=f_2(\mathrm{SOC},I)>0 \quad [\mathrm{m^2\cdot\Omega/s}] \tag{13}$$

In summary, (3)–(13) describe the complete Li-ion cell model with the four state variables: $c^+_{s,\mathrm{avg}}(t)$, $c^-_{s,\mathrm{avg}}(t)$, $r_f(t)$ and $Q_{\max}(t)$. Note that SOC$^{\pm}$, $x^{\pm}_{s,\mathrm{avg}}$, $x^{\pm}_{\mathrm{ss}}$, and $c^{\pm}_{\mathrm{ss}}$ may also be selected as state variables, considering the linear relationships given in (3), (4) and (11).

Additionally, the battery cell temperature is assumed to be effectively regulated to a constant value, so the thermodynamic model of the cell is not incorporated. Assuming identical cells, cell model can be scaled up to the pack-level. The battery pack power $P_b(t)$ as shown in Fig. 1 is

$$P_b(t)=-n_{\mathrm{cell}}V(t)I(t)\times10^{-3} \quad [\mathrm{kW}] \tag{14}$$

where n_{cell} is the number of cells. The minus sign in (14) indicates that the direction of pack power $P_b(t)$ is defined opposite to the cell current $I(t)$.

D. Electricity Tariff

In this study, it is assumed that the prosumer is allowed to autonomously determine the dispatched power P_d. The prosumer is to trade P_d so as to minimize the operating cost to the prosumer. Such trading of P_d can bring income to the prosumer through exporting P_d to the grid. This will incentivize the prosumer to engage in the active control of the network within its purview.

To simplify analysis, it is assumed the same electricity tariff applied to the exporting and importing of P_d. Variations in tariff can be readily included in the study, if the tariff structure is known. Furthermore, it is assumed the DSO is to provide the prosumer the short-term forecast ($\lambda_f(t)$) of the spot price of electricity. An example of half-hourly actual and forecasted electricity tariffs $\lambda(t)$ and $\lambda_f(t)$ respectively are shown in Fig. 3. The data was modified from the wholesale spot price provided by the Australian Energy Market Operator (AEMO).

III. Determination of the Dispatch

A. Market Rules on P_d

In this study, it is assumed the market rule for the prosumer is similar to that applicable for a large-scale renewable generator [11]. According to such rule, the prosumer is to submit to the DSO the D-hour dispatch schedule R hours ahead. The schedule contains the power level over each dispatch interval T and at specified set time. However, the prosumer is allowed to alter the submitted schedule except for the immediate Y hours. This rule is illustrated in Fig. 4 for time t.

According to the rule, the dispatch schedule from time $t + R$ to $t + H$ (denoted by the blue dashed line, where $H = R + D$) must be submitted to the DSO at time t. The dispatch schedule from t to $t + Y$ has been determined before t (denoted by the red solid line) and cannot be altered. While the schedule from $t + Y$ to $t + R$ has been submitted before t, the schedule over this interval can be revised and resubmitted together with that over the interval $t + R$ to $t + H$ at t.

B. Prediction Model

The proposed control strategy will use MPC technique to determine the optimal power flow P_d at the point of coupling (POC) shown in Fig. 1. Using system model (1)–(14), the prediction model can be expressed in the state-space form, i.e.

$$\dot{x}(t)=f(x(t),u(t),d(t)) \tag{15}$$

where the state variables are selected as $x(t)$ = [SOC$^+(t)$, SOC$^-(t)$, $Q_{\max}(t)$, $r_f(t)$], control variable $u(t) = P_d(t)$, disturbance $d(t)$ = [$P_{\mathrm{PV},f}(t)$, $P_{L,f}(t)$, $\lambda_f(t)$]. In current work, the comfort level of the prosumer is of the highest priority and it is assumed that there is no deferrable load.

As such, within the prediction horizon H, the control objective is to minimize the overall operating cost to the prosumer. The cost would include the income from the trading of electricity and the cost incurred due to the degradation in the battery. It is meaningful to include the cost of the battery degradation in the evaluation because the lifetime of battery is expected to be lower than that of the PV generator. Other objectives, such as the emission level, can be readily

incorporated into the presented framework if the corresponding cost models are available.

The income from the trading of electricity is given by

$$C_1(t) = -P_d(t)\lambda(t) \quad [\$/\mathrm{h}] \tag{16}$$

Thus a negative value of C_1 means that the prosumer has obtained a net gain from the cost of electricity trading and vice versa. The cost due to battery degradation is related to the capacity fading rate $\dot{Q}_{\max}(t)$. This cost component can be expressed as:

$$C_2(t) = -\frac{n_{\text{cell}} C_b}{(1-K\%)Q_{\max,0}} \dot{Q}_{\max}(t) > 0 \quad [\$/\mathrm{h}] \tag{17}$$

where $\dot{Q}_{\max}(t)$ is governed by (12). C_b is the capital cost per cell, thus $n_{\text{cell}}C_b$ is the total cost of the battery packs. K% defines the percentage of the remaining capacity of the packs when the packs are considered to be at the end of their service life. The value of K% is assumed known. As the capacity fading rate is always negative, $C_2(t)$ is always positive.

In view of the above and within the time interval $[t, t+H]$, the objective cost function J can be expressed as

$$J(u(t)) = \int_{t}^{t+H} \left[\alpha C_1(\tau) + \beta C_2(\tau)\right] d\tau \tag{18}$$

The weighting factors $\alpha, \beta \in [0, 1]$ can be set in accordance to the purpose of latter analysis. As (18) represents the overall cost to the prosumer over H, the objective is to minimize J.

Considering the practical limits of the components in the system, the following inequality constraints are applicable:

$$\begin{aligned} -P_{b,\max} &\le P_b(t) \le P_{b,\max} \\ -P_{d,\max} &\le P_d(t) \le P_{d,\max} \\ \mathrm{SOC}_{\min} &\le \mathrm{SOC}(t) \le \mathrm{SOC}_{\max} \end{aligned} \tag{19}$$

where $P_{b,\max}$ and $P_{d,\max}$ are the power ratings of the battery converter and the interface transformer respectively. $\mathrm{SOC}_{\min}$ and $\mathrm{SOC}_{\max}$ are the lower and the upper SOC limits of the battery. They are included in (19) to prevent permanent damage to the battery cells caused by overdischarge and overcharge respectively.

As the first Y hours' schedule is determined in the previous prediction horizon and cannot be changed, the following constraints are used to reflect this market rule, i.e.

$$P_d(\tau) = \begin{cases} P_{d,opt}(\tau), & t \le \tau < t+T \\ P_{d,opt}(\tau+T), & t+T \le \tau < t+2T \\ \ldots & \ldots \\ P_{d,opt}(\tau+Y-T), & t+Y-T \le \tau < t+Y \end{cases} \tag{20}$$

where $P_{d,\text{opt}}(.)$ represents the optimal dispatch schedule determined in the previous prediction horizon $[t–T, T]$.

Additionally, the following constraint signifies constant dispatch within each dispatch internal T, i.e.

$$P_d(t) = P_d(\lfloor t/T \rfloor \times T) \tag{21}$$

where $\lfloor t \rfloor$ is the largest integer that does not exceed t.

C. Model Predictive Control

To implement MPC, the continuous-time model (15) and the objective cost function (18) as well as the constraints (19)–(21) must first be discretized in the time domain using the selected time-step T_s (expressed in second in this study). According to the classical theory of MPC, the discrete optimal dispatch power sequence $P_{d,k}$ (where the integer k is the time step index) can be determined via the following steps:

Step 1: Obtain the discretized forecasted PV panel power $P_{\text{PV},f,k}$, forecasted load $P_{L,f,k}$, and forecasted electricity price $\lambda_{f,k}$. The prediction horizon (number of discrete points for optimization) is $N = 3600H/T_s$;

Step 2: Compute the optimal control sequence $P_{d,\text{opt},k}$ by solving the optimization problem. In the next sub-section, more will be said about the optimization method used;

Step 3: Only apply the optimal control sequence in the next dispatch interval T to the system model. The number of discrete points within one dispatch interval is $n = 3600T/T_s$.

Step 4: Forward the prediction horizon by one dispatch interval T: Measure the resulting system states, update system constraints and the forecasted disturbances, and repeat the above procedure starting from the time corresponding to the $(k + n)^{\text{th}}$ time step.

D. Modified DP

In *Step 3*, due to the high-nonlinearity of the system model (1)–(14), DP technique will be used to solve this constrained nonlinear optimization problem. However, conventional DP suffers from the "curse of dimensionality" problem: the computation load increases exponentially as the number of the state variables. The fourth-order battery model will incur long computation time. To obviate this problem, a new algorithm is now proposed to speed up the optimization process. Considering that the degradation process described by (12) and (13) is much slower than the charging process described by (3)–(11), *Step 2* and *Step 3* will be modified to:

Step 2 (modified): keep the slow-varying variables $Q_{\max}$ and r_f in (10) and (6) constant and use DP to obtain the optimal control input sequence $P'_{d,\text{opt},k}$. As only two states are needed for DP, the computational load can be significantly reduced. The discretized objective cost function is thus

$$J_k(P_{d,k}) = \sum_{i=k}^{k+N-1} \left\{ -\alpha P_{d,i}\lambda_i - \beta \frac{n_{\text{cell}} C_b \dot{Q}_{\max,i}}{(1-K\%)Q_{\max,0}} \right\} \tag{22}$$

Step 3 (modified): Only apply the first n-step of the optimal control sequence $P'_{d,\text{opt},k}$ to the original model (1)–(14). In this way all the four state-variables including r_f and $Q_{\max}$ can be updated.

E. Two Measures on Cost

The effectiveness of the control strategy can be evaluated using the total cost (TC) or the average cost (AC). TC at time step k can be calculated by summating all the cost incurred since the initial time step $k = 1$, i.e.

$$\mathrm{TC}_k = \sum_{i=1}^{k} \left(-P_{d,i}\lambda_i - \frac{n_{\text{cell}} C_b \dot{Q}_{\max,i}}{(1-K\%)Q_{\max,0}} \right) \frac{T_s}{3600} \quad [\$] \tag{23}$$

The AC at time step k can be defined as the TC per unit time (say per day), i.e.

$$\mathrm{AC}_k = \frac{\mathrm{TC}_k}{kT_s/(3600\times 24)} \qquad [\$/\mathrm{Day}] \qquad (24)$$

IV. Illustrative Examples and Discussions

A. Contributions of Electricity Trading and Battery Degardation Costs

The following parameters are used in the simulation study: $Q_{\max 0}$ = 1.74 Ah, C_b = \$4, K% = 60%, n_{cell} = 6000. Prediction horizon H = 24 h, dispatch interval T = 1 h, Y = 2 h, T_s = 300 s.

The weighting factors in (18) represent how much emphasis is placed on the income obtained from the trading of electricity and the cost of battery degradation. When α = 1 and β = 0, battery degradation is not considered for the optimization and only the net income of trading electricity is considered; conversely, for α = 0 and β = 1, the cost of battery degradation is the only concern. For α = 1 and β = 1, trading and degradation are considered concurrently. A 24-hour simulation result for the three cases are shown in Fig. 5.

From Fig. 5, it can be seen that with the trading-emphasized strategy, the dispatch and battery power changes most drastically in response to the price fluctuations, but such changes will speed up the battery degradation due to the high power/current generated. On the other hand, for the degradation-emphasized strategy, less power is applied to the battery so its lifetime can be most effectively prolonged. However, less income can be gained from the trading of the electricity. When the trading and degradation are considered concurrently, the highest economic benefit can be obtained. This is verified by observing the TC values after one-day operation (which numerically equals to AC) in Fig. 5(*f*): i.e. – \$2.325, –\$0.747 and –\$2.985 for the three cases respectively. Also, in this particular short-duration study, it shows that the prosumer has secured a net gain from the optimized operation.

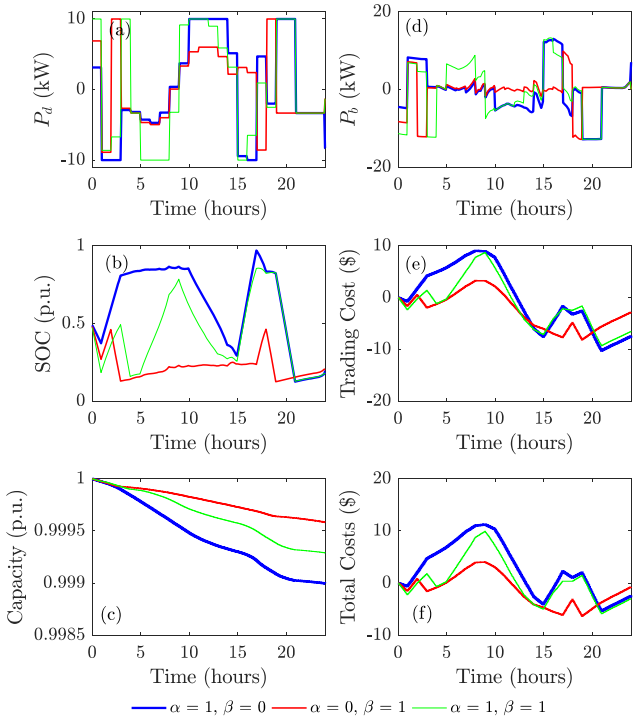

Fig. 5. 24-hour simulation results for: trading-emphasized (blue), degradation-emphasized (red) and when both factors are concurrently emphasized (green).

B. Longer Term Electricity Trading and Battery Degardation Costs

The simulation results for a 32-day operation are shown in Fig. 6. From Fig. 6 (c), it can be seen that for the three cases described in Section IV-A, TCs are, \$181.8, \$240.2 and \$162.5 after one month, and the corresponding ACs are \$5.68/day, \$7.51/day and \$5.07/day. This shows that the proposed MPC can indeed bring economic benefits to the prosumer by considering the electricity trading and battery degradation at the same time, although the prediction horizon is much smaller than the total simulation time. In this case, the total costs can be saved by more than 10% compared to the case without considering the battery degradation. Additionally, it shows that although in the 1-day operation considered in Section IV.A in which the user can obtain a net gain, for the longer term operation shown in this section has resulted in a net loss to the prosumer.

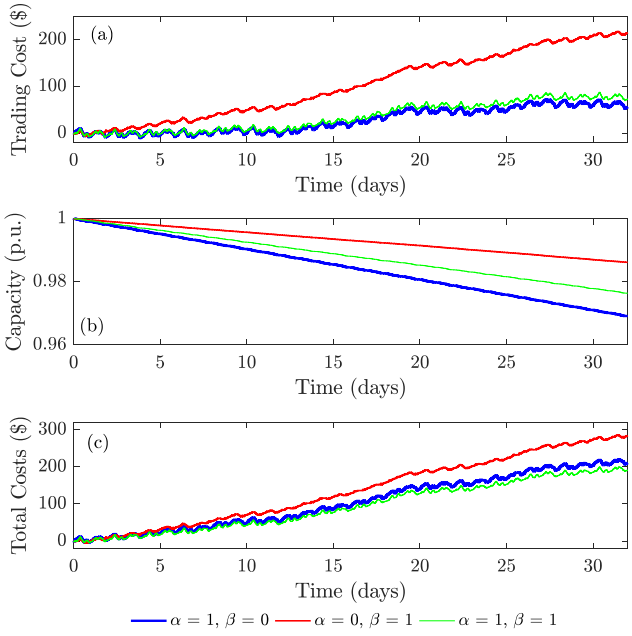

Fig. 6. 32-day simulation results for: trading-emphasized (blue), degradation-emphasized (red) and when both factors are concurrently emphasized (green).

C. Performance Under Different BESS Capacity

Fig. 7 shows the trading costs, battery degradation cost and the average costs when the BESS of 4,000 cells or 6,960 Ah, 6,000 cells or 10,440 Ah and 8,000 cells or 13,920 Ah capacities are assumed. As can be seen from Fig. 7(a) and (b), smaller BESS capacity will incur higher trading cost while larger BESS capacity will incur higher battery costs due to degradation. From Fig. 7(c), it can be seen that the average costs fluctuate significantly at the beginning of the simulation and it can go negative. AC becomes more stable with time. Thus, in order to evaluate the economic effectiveness, long term study is more

reasonable. Additionally, it can be clearly seen that $n_{cell} = 6000$ will cost least amongst these three cases.

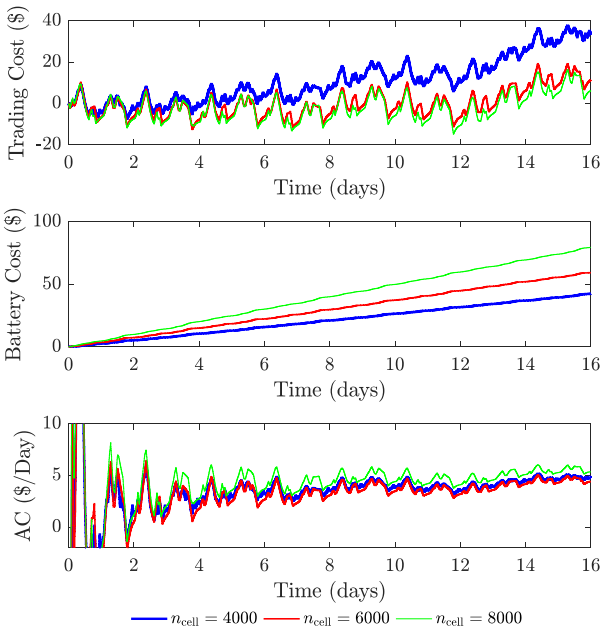

Fig. 7. Trading costs, battery costs due to degradation and average costs for BESS of 4000x1.74 Ah (blue), 6000x1.74 Ah (red) and 8,000x1.74 Ah (green).

V. Conclusions

This paper proposes a general approach to determine the optimal control strategy for a prosumer equipped with PV and Li-ion battery under the dynamic energy market environment. The control objective is to minimize the overall cost to the prosumer while meeting the electrical demand of the prosumer. Nonlinear model predictive control technique is used to determine the optimal power exchange with the grid. Considering the highly nonlinear nature of the lithium-ion battery, the optimization problem is formulated and dealt with using a much simplified dynamic programming approach. From the study, it appears that in designing the dispatch strategy, the battery degradation cost has to be included in the cost evaluation. The developed Li-ion battery model is such that short-term dispatch strategy for the prosumer can be determined in real-time.

Acknowledgment

This work was supported by the Australian Research Council Discovery Grant DP160101325.

Appendix A

The Li-ion cell electrochemical parameters and OCP vs. stoichiometry equations are obtained from [9] with minor adaptation of ε_s, $x_{0\%}$, and $x_{100\%}$.

Sym-bol	Physical meaning [Unit]	Parameters	
		+	–
R_p	particle radius ($\times 10^{-6}$ m)	2	2
D_s	diffusion coefficient in the solid phase ($\times 10^{-14}$ m^2/s)	1	3.9
a	specific surface area of electrode ($\times 10^5$ m^{-1})	8.85	7.236
L	length of the electrode ($\times 10^{-6}$ m)	80	88
ε_s	volume fraction of the solid phase	0.59	0.4824
$c_{s,\max}$	theoretical maximum Li-ion concentration in the solid phase (mol/m^3)	51554	30555
$x_{0\%}$	stoichiometry at SOC = 0%	0.9433	0.0117
$x_{100\%}$	stoichiometry at SOC = 100%	0.4938	0.8551
r_{eff}	electrode rate constant ($\times 10^{-6}$ A·m$^{2.5}$·mol$^{-1.5}$)	2.252	4.854
F	Faraday's constant (s·A/mol)	96485	
T_{cell}	temperature (K)	298	
R_g	universal gas constant [J/(K·mol)]	8.31446	
r_{col}	current collector resistance (Ω·m^2)	0.002	
c_{e0}	average Li-ion concentration in the electrolyte (mol/m^3)	1000	
A_{cell}	electrode plate area (m^2)	0.0596	

$$\mathrm{OCP}^{+}(x^{+}) = \frac{-a_0 + a_1(x^{+})^2 - a_2(x^{+})^4 + a_3(x^{+})^6 - a_4(x^{+})^8 + a_5(x^{+})^{10}}{-b_0 + b_1(x^{+})^2 - b_2(x^{+})^4 + b_3(x^{+})^6 - b_4(x^{+})^8 + b_5(x^{+})^{10}}$$

$$\mathrm{OCP}^{-}(x^{-}) = c_0 + c_1(x^{-}) + c_2(x^{-})^{0.5} - c_3(x^{-})^{-1} + c_4(x^{-})^{-1.5} +$$

$$+c_5 \exp(c_6 - c_7(x^{-})) - c_8 \exp(c_9(x^{-}) - c_{10})$$

$a_0 = 4.656$, $a_1 = 88.669$, $a_2 = 401.119$, $a_3 = 342.909$, $a_4 = 462.471$, $a_5 = 433.434$; $b_0 = 1$, $b_1 = 18.933$, $b_2 = 79.532$, $b_3 = 37.311$, $b_4 = 73.083$, $b_5 = 95.96$; $c_0 = 0.7222$, $c_1 = 0.1387$, $c_2 = 0.029$, $c_3 = 0.0172$, $c_4 = 0.0019$, $c_5 = 0.2808$, $c_6 = 0.90$, $c_7 = 15$, $c_8 = 0.7984$, $c_9 = 0.4465$, $c_{10} = 0.4108$.

References

[1] "Small-scale renewable energy hits record-breaking capacity in Australia," *Australian Government Clean Energy Regulator News and Updates*, 2017, [Online]. Available: http://www.cleanenergyregulator.gov.au/About/Pages/News%20and%20updates/NewsItem.aspx?ListId=19b4efbb-6f5d-4637-94c4-121c1f96fcfe&ItemId=417

[2] M. Karimi, H. Mokhlis, K. Naidu, S. Uddin, and A. H. A. Bakar, "Photovoltaic penetration issues and impacts in distribution network – a review," *Renew. Sustain. Energy Rev.,* vol. 53, pp. 594-605, Jan. 2016.

[3] M. C. Bozchalui, S. A. Hashmi, H. Hassen, C. A. Canizares, and K. Bhattacharya, "Optimal operation of residential energy hubs in smart grids," *IEEE Trans. Smart Grid,* vol. 3, no. 4, pp. 1755-1766, Dec. 2012.

[4] O. Erdinc, N. G. Paterakis, T. D. P. Mendes, A. G. Bakirtzis, and J. P. S. Catalão, "Smart household operation considering bi-directional EV and ESS Utilization by real-time pricing-based DR," *IEEE Trans. Smart Grid,* vol. 6, no. 3, pp. 1281-1291, Sep. 2015.

[5] C. Sun, F. Sun, and S. J. Moura, "Nonlinear predictive energy management of residential buildings with photovoltaics & batteries," *J. Power Sources,* vol. 325, no. Supplement C, pp. 723-731, Sep. 2016.

[6] M. Diagne, M. David, P. Lauret, J. Boland, and N. Schmutz, "Review of solar irradiance forecasting methods and a proposition for small-scale insular grids," *Renew. Sustain. Energy Rev.,* vol. 27, pp. 65-76, Nov. 2013.

[7] Z. Ziadi, *et al.*, "Optimal voltage control using inverters interfaced with PV systems considering forecast error in a distribution system," *IEEE Trans. Sustain. Energy,* vol. 5, no. 2, pp. 682-690, Apr. 2014.

[8] Y. Li, D. M. Vilathgamuwa, T. W. Farrell, S. S. Choi, and N. T. Tran, "An equivalent circuit model of Li-ion battery based on electrochemical principles used in grid-connected energy storage applications," in *IEEE 3rd Int. Future Energy Electron. Conf. & ECCE Asia*, Kaohsiung, Taiwan, 3-7 Jun. 2017, pp. 959-964.

[9] P. Ramadass, B. Haran, P. M. Gomadam, R. White, and B. N. Popov, "Development of first principles capacity fade model for Li-ion cells," *J. Electrochem. Soc.,* vol. 151, no. 2, pp. A196-A203, Jan. 2004.

[10] Y. Li, *et al.*, "Optimal control of film growth in dual lithium-ion battery energy storage system," in *12th IEEE Int. Conf. Power Electron. Drive Syst. (PEDS 2017)*, Honolulu, HI, USA, 12-15 Dec. 2017, pp. 202-207.

[11] Y. Li, S. S. Choi, D. M. Vilathgamuwa, and D. L. Yao, "An improved dispatchable wind turbine generator and dual-battery energy storage system to reduce battery capacity requirement," in *Proc. IEEE Annu. Southern Power Electron. Conf. (SPEC)*, Auckland, New Zealand, 5-8 Dec. 2016, pp. 1-6.